Journal of Medicinal Chemistry

ARTICLE

pubs.acs.org/jmc

Synthesis, Activity, and Structural Analysis of Novel α-Hydroxytropolone Inhibitors of Human Immunodeficiency Virus Reverse Transcriptase-Associated Ribonuclease H

Suhman Chung,[†,⊥] Daniel M. Himmel,[‡,⊥] Jian-Kang Jiang,[§] Krzysztof Wojtak,[‡] Joseph D. Bauman,[‡] Jason W. Rausch,[†] Jennifer A. Wilson,[∥] John A. Beutler,[∥] Craig J. Thomas,[§] Eddy Arnold,[‡] and Stuart F.J. Le Grice*[,†]

[†]RT Biochemistry Section, HIV Drug Resistance Program, National Cancer Institute—Frederick, Frederick, Maryland 21702, United States

[‡]Center for Advanced Biotechnology and Medicine and Department of Chemistry and Chemical Biology, Rutgers University, Piscataway, New Jersey 08854, United States

[§]NIH Chemical Genomics Center, Rockville, Maryland 20850, United States

[∥]Molecular Discovery Program, National Cancer Institute—Frederick, Frederick, Maryland 21702, United States

ABSTRACT: The α-hydroxytroplone, manicol (5,7-dihydroxy-2-isopropenyl-9-methyl-1,2,3,4-tetrahydro-benzocyclohepten-6-one), potently and specifically inhibits ribonuclease H (RNase H) activity of human immunodeficiency virus reverse transcriptase (HIV RT) in vitro. However, manicol was ineffective in reducing virus replication in culture. Ongoing efforts to improve the potency and specificity over the lead compound led us to synthesize 14 manicol derivatives that retain the divalent metal-chelating α-hydroxytropolone pharmacophore. These efforts were augmented by a high resolution structure of p66/p51 HIV-1 RT containing the nonnucleoside reverse transcriptase inhibitor (NNRTI), TMC278 and manicol in the DNA polymerase and RNase H active sites, respectively. We demonstrate here that several modified α-hydroxytropolones exhibit antiviral activity at noncytotoxic concentrations. Inclusion of RNase H active site mutants indicated that manicol analogues can occupy an additional site in or around the DNA polymerase catalytic center. Collectively, our studies will promote future structure-based design of improved α-hydroxytropolones to complement the NRTI and NNRTI currently in clinical use.

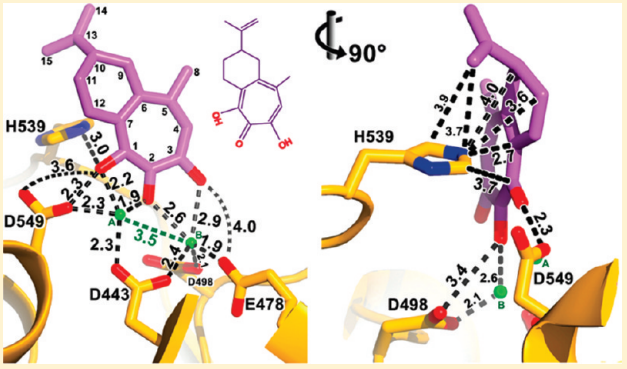

INTRODUCTION

Synthesis of double-stranded, integration-competent DNA in retroviruses proceeds through an RNA/DNA hybrid intermediate, whose (+) RNA genome must be removed to facilitate second, or (+)-strand, DNA synthesis.[1] Hybrid hydrolysis is mediated by the C-terminal RNase H domain of the virus-coded reverse transcriptase (RT). RT of human immunodeficiency virus (HIV), the etiological agent of acquired immunodeficiency syndrome (AIDS), is a p66/p51 heterodimer of asymmetrically organized subunits processed from the 165 kDa *gag/pol* polyprotein precursor.[2,3] Abrogating RNase H function was demonstrated almost two decades ago to inhibit enzyme activity in vitro and virus replication in culture,[4,5] thereby demonstrating that RNase H antagonists might be combined with nucleoside and nonnucleoside RT inhibitors currently in clinical use as components of highly active antiretroviral therapy (HAART). Since these early reports, however, there been a paucity of data on clinical trials with small molecule RNase H inhibitors, possibly reflecting their toxicity, lack of selectivity, or poor cellular penetration.

Development of HIV RNase H inhibitors has recently been encouraged by documentation of several structurally dissimilar classes of antagonists derived from natural products or via chemical synthesis. Examples of the former include the α-hydroxytropolones,[6,7] dimeric lactones,[8] madurahydroxylactones,[9] and 1,3,4,5-tetragalloylapiitol[10] (Figure 1), while synthetic entities include *N*-hydroxyimides, diketo acids, pyrimidinol carboxylates,[11] vinylogous ureas,[12,13] thiocarbamates, and triazoles.[14] While many of these compounds target the RNase H active site, our recent work suggests that vinylogous ureas represent a class of allosteric inhibitors that influence RNase H active site geometry by binding to the p51 thumb subdomain.[13] In addition to this expanding collection of small molecules, X-ray crystallography has provided high resolution information on enzyme:inhibitor complexes with either the isolated RNase H domain or the intact p66/p51 heterodimer,[11,15−18] which should aid future structure-based efforts.

Received: January 24, 2011
Published: May 13, 2011

ACS Publications © 2011 American Chemical Society

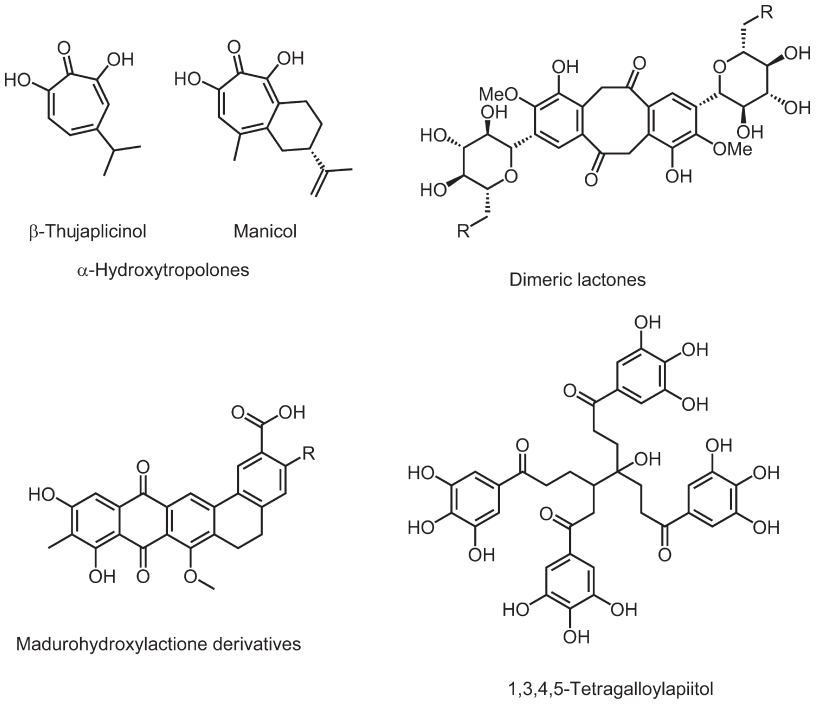

Figure 1. Chemical structures of HIV-1 RNase H inhibitors derived from natural products.

Although potently and selectively inhibiting RNase H activity of HIV-1 and HIV-2 RT, the natural products, β-thujaplicinol (2,7-dihydroxy-4-isopropyl-cyclohepta-2,4,6-triene) and manicol (5,7-dihydroxy-2-isopropenyl-9-methyl-1,2,3,4-tetrahydrobenzocyclohepten-6-one), were ineffective in reducing virus replication in culture, most likely due to toxicity caused by inhibition of cellular enzymes.[19] To overcome the toxicity issue and improve potency and selectivity, our efforts have been focused on derivatization of these inhibitors. Our previous structure−activity relationship studies showed that three oxygen ligands of inhibitors are critical while substitutions elsewhere on the heptatriene ring were less deleterious.[6] Indeed, epoxidation of the alkene moiety of manicol did not interfere with the biological activity (IC_{50} = 0.45 μM). This terminal alkene was therefore chosen as a target site for modification because of its versatile chemistry. The synthesis, in vitro evaluation, and antiviral activity of 14 novel manicol derivatives are the subject of this communication. In addition to providing the first report of α-hydroxytropolones with antiviral activity against HIV-1, we present here the high resolution crystal structure of p66/p51 HIV-1 RT containing the NNRTI, **18** (TMC278)[20] in the DNA polymerase domain and manicol complexed with divalent metal at the RNase H active site. Interestingly, the bound structure of manicol differs in conformation from that of the bulk manicol structure reported by Polonsky et al.[21] The high resolution cocrystal structure, together with our revised manicol structure, will allow us to develop future generations of RNase H inhibitors with greater selectivity, as well as examine the effect of simultaneous application of DNA polymerase and RNase H inhibitors on HIV replication.

RESULTS

Structure of HIV-1 RT Containing Manicol and the NNRTI, 18. Although a high resolution structure for HIV-1 RT containing β-thujaplicinol was recently solved,[15] the related natural product, manicol, is more readily amenable to modification because it possesses a double bond in its side chain. To guide synthesis of future α-hydroxytropolones, we therefore solved the structure of p66/p51 HIV-1 RT containing **18** in the DNA polymerase domain and manicol at the RNase H active site. The structure, refined at 2.7 Å resolution (Table 1), revealed unambiguous electron density maps for manicol binding (Figure 2). Two strong Mn^{2+} peaks in the electron density map within the RNase H active site and correspond to the divalent cation positions "A" and "B" (following the convention for a two-cation mechanism of hydrolysis[22,23]). The carbonyl oxygen and both hydroxyls of the tropolone ring coordinate the divalent cations in a manner similar to that previously observed in the RT/β-thujaplicinol structure.[15]

Unlike β-thujaplicinol, manicol forms extensive contacts with the imidazole ring of His539 (Figure 3a), including contacts with interatomic distances of under 3 Å. Because tropolone ring systems can have aromatic character,[24] the His539-manicol interaction is an example of an aromatic−aromatic interaction. As reviewed in refs 25−27, interactions between the imidazole side chain of histidine and another aromatic ring has been documented in a number of configurations. These include parallel stacking of the aromatic rings and edge-on-face orientations, in which a histidine C/N−H serves as a hydrogen-bonding donor. While in many cases the histidine C/N−H points toward the center of the other aromatic ring, there are examples in which the imidazole ring edge is offset from the center of the other ring, as seen in the His539−manicol interaction. Conventionally, to be considered a hydrogen-bonding interaction, the angle between C/N−H to the center of the aromatic ring should be greater than 120° and the distance between the C/N and the ring should be less than 3.5 Å. Both criteria are satisfied in the His539−manicol interaction

At 2.7 Å resolution, we cannot completely rule out an alternative possibility. Tropolone rings are believed to behave

dx.doi.org/10.1021/jm2000757 |J. Med. Chem. 2011, 54, 4462–4473

Table 1. Data Collection and Refinement Statistics for p66/p51 HIV-1 RT/18/Manicol Cocrystal

(a) Unit Cell Parameters (Space Group C2)	
a (Å)	163.9
b (Å)	73.0
c (Å)	108.4
β (Å)	101.1
(b) Data Collection	
resolution range (Å)	45−2.7
R_{sym}(%)	6.3
average I/σ	16.1
completeness (%)	99.5
unique reflections/multiplicity:	34841/6.2
(c) Refinement	
σ cutoff	0.0
resolution range used (Å)	45−2.7
completeness of used reflections (%)	95.8
R-factor/R_{free} (%)	23.2/25.1
cross-validated coordinate error (Å)[24]	0.36
no. of protein/solvent atoms	7907/96
no. of ligand/cation atoms	54/2
average B-factors (Å^2)	
protein/solvent	76.7/60.3
ligands/cations	77.5/68.0
rms bond lengths (Å)/angles (deg)[53]	0.010/1.27
(d) Ramachandran Regions	
most favored	95.0
additional allowed	4.2%
generous or disallowed	0%

as electron-deficient aromatic rings ("tropylium"), as discussed in ref 15. If manicol forms a tropylium ion, then the tropolone ring carries a positive charge, while the three oxygens may share a resonant negative charge that contributes to the coordination of the two observed Mn^{2+} cations at the RNase H active site. These circumstances raise the question of whether His539 may serve as a Lewis base, in which one of the lone pair electrons of nitrogen atom serves as an electron donor to the delocalized positive charge of the tropolone ring and stabilizes the tropylium ion, analogous to anion−π interactions that have recently been reported both in small organic molecule and biological structures.[28,29] In this case, we suspect that proximity of His539 to the manicol ring system would produce excessive electronegative repulsion if not mediated by a hydrogen-bonding proton.

The electron density clearly indicates that the alicyclic carbon atoms of manicol pucker in the direction of the His539 side chain, with the 2-isopropenyl substituent occupying the equatorial position on the C10 carbon. This observation is in contrast to a previous small molecule crystal structure study of Polonsky et al.[21] which reported that the 2-isopropenyl substituent occupied the axial orientation (Figure 3b). In both our results and the Polonsky et al. study, the chiral center at the C10 carbon has an *S* configuration. In the RT/β-thujaplicinol structure,[15] one hydroxyl group of the tropolone ring came within hydrogen bonding distance of the side chain carboxylates of the catalytically essential residues Glu478 and Asp498. Significantly, manicol pivots away from these residues and loses these interactions in favor of contacts with His539 and a 2.4 Å contact between one of the tropolone hydroxyls and the side chain carboxylate of Asp549. Manicol does, however, retain hydrophobic interactions with Glu478 and Asp498 (contact distances ranging from 3.4 to 4.0 Å).

Other structures of either the p66/p51 RT heterodimer or the isolated 15 kDa HIV RNaseH domain have recently been published in which an RNase H inhibitor has been demonstrated to occupy the RNase H active site by coordinating two active site Mn^{2+} cations. These include β-thujaplicinol,[15] a pyrimidinol carboxylic acid derivative,[11] and several naphthyridinone derivatives.[18] Su et al. observed that most of these compounds position their metal-coordinating moieties in approximately the same plane with the metal ions.[18] It was therefore suggested that it might be helpful to design RNase H inhibitors on the assumption that the metal-chelating moiety would lie in the same plane with the metals. However, one of the naphthyridinone derivatives, MK3, was not coplanar with the Mn^{2+} cations in these studies. Likewise, when comparing manicol to β-thujaplicinol, we observe that, while the tropolone ring of the latter is essentially coplanar with the metal cations, the manicol counterpart is not. The full significance of this observation is not clear but may be related to the favorable interactions that manicol can form with the His539 side chain if the tropolone ring moves out of the plane of the metal cations. Another possible contributing factor could be the molecular orbital alignment of the outer shell electrons about the central tropolone oxygen as it chelates both Mn^{2+} cations. If that oxygen behaves predominantly like a carbonyl, in which the outer shell electrons form sp^2 hybrid orbitals and a π-orbital, then the lone pair electrons that coordinate the Mn^{2+} cations might be expected to favor a trigonal planar arrangement. Conversely, if the oxygen carries a formal negative charge, in which the outer shell electrons predominantly form sp^3 hybrid orbitals, then a roughly tetrahedral (nonplanar) geometry might be favored for the lone pair electrons that coordinate the cations.

Manicol Derivatization. The synthesis of manicol analogues is depicted in Scheme 1. Manicol epoxide **16** was synthesized according to the reported procedure.[21] In vitro studies indicated that manicol epoxide retained its efficacy as an RNase H inhibitor. Opening of epoxide **16** with a variety of amines catalyzed by stoichiometric $LiClO_4$ afforded analogues **1**−**5**. Addition of selected thiols required Et_3N or NaH and resulted in sulfides **6**−**8**. Sulfides **6** and **7** were oxidized with *m*-CPBA to either sulfoxide **10** or sulfones **9** and **11** by adjusting the reaction temperature. Starting from diacetyl-protected manicol intermediate **15**, dihydroxylation of the olefin functionality using OsO_4/NMO followed by the deprotection of the acetyl groups gave analogue **12**. Alternatively, in the presence of OsO_4 and $NaIO_4$, the in situ dihydroxylation/oxidative cleavage of **15** furnished ketone **17**, which could be reduced to alcohol **13** with $NaBH_4$ or converted to amine **14** via reductive amination. It should be noted that all of the tested analogues (**1**−**14**) were obtained as a mixture of stereoisomers.

In Vitro Inhibition of RNase H Activity. Using a previously reported high throughput, fluorescence-based RNase H assay,[30] Table 2 provides the IC_{50} values for compounds **1**−**14**. Compound **9** was slightly more potent than manicol (IC_{50} 0.24 μM vs 0.6 μM, respectively), while a 3−4-fold decrease in activity was observed for compound **2** (IC_{50} 1.9 μM). All remaining compounds fell within this range. Because the high throughput

dx.doi.org/10.1021/jm2000757 |J. Med. Chem. 2011, 54, 4462–4473

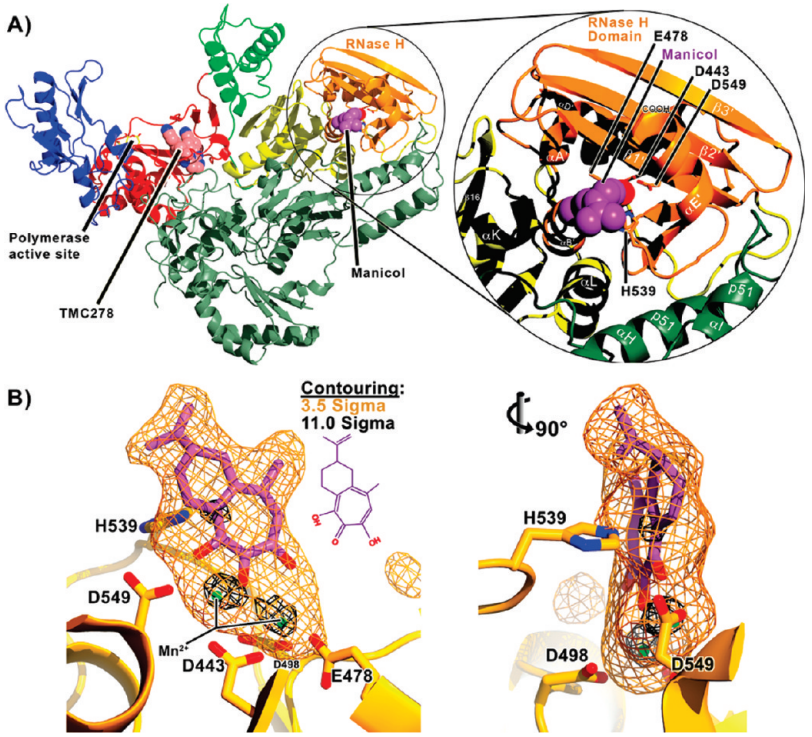

Figure 2. Structure of HIV-1 RT containing the NNRTI, **18** and manicol. (A) A ribbon diagram of the structure of RT in complex with both **18** (pink) and manicol (violet). RT is a heterodimer comprising p66 (in color) and p51 (gray) subunits. The subdomains of p66 are shown in color as indicated. Right inset: a close-up view of the RNase H domain and nearby secondary structural elements. Helices and β-sheets are labeled according to reference.[53] Side chains for the RNase H active site carboxylates (D443, E478, H539, and D549) are shown. (B) Manicol at the RNase H active site. A simulated annealing $F_o - F_c$ electron density omit map is shown in which manicol and two Mn^{2+} cations have been omitted from the phasing. The map is contoured both at the 3.5 σ (orange) and 11.0 σ (black) levels. The manicol molecule modeled into this density is shown with its carbon atoms in violet. Two different vantage points are shown rotated 90° from each other about the vertical axis. The inset (center top) gives the chemical structure of manicol.

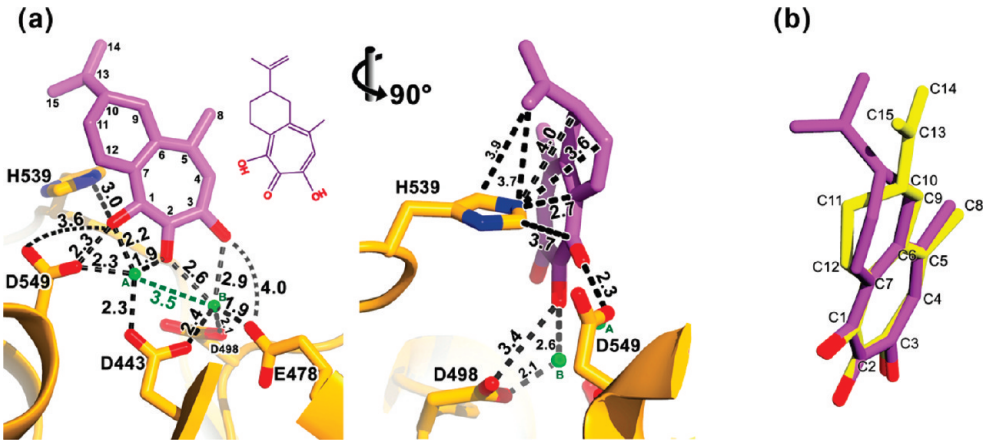

Figure 3. (a) Interaction distances (dashed lines, Å) between manicol (magenta carbon atoms), two Mn^{2+} cations (green), and RT. The same vantage points are shown as in Figure 1b. Divalent cations are labeled A and B following the convention for a two-cation mechanism of hydrolysis. Numbering for the manicol carbon atoms is shown (black, left image). Most of the close contacts that manicol forms with RT are with amino acid residue His539. (b) Comparison of manicol conformations. The manicol conformation we observed (yellow carbon atoms) is superimposed on a conformation reported from a small molecule crystallization study of manicol[21] (magenta carbon atoms). The carbon numbering used in the deposited PDB coordinates is shown. We find that the alicyclic carbons pucker in the opposite direction than previously reported.

RNase H assay examines nonspecific, "polymerase-independent" RNase H activity defined by the spatial separation of the DNA polymerase and RNase H active site of HIV-1 RT,[31] we examined whether α-hydroxytropolones altered cleavage specificity on a more biologically relevant substrate, namely the polypurine tract (PPT) primer, which must be processed from the RNA/DNA replication intermediate to initiate (+) strand DNA synthesis.[1] Inhibition of RNase H activity on this model PPT-containing

dx.doi.org/10.1021/jm2000757 |J. Med. Chem. 2011, 54, 4462–4473

Scheme 1. Syntheses of Manicol Derivatives 1−14[a]

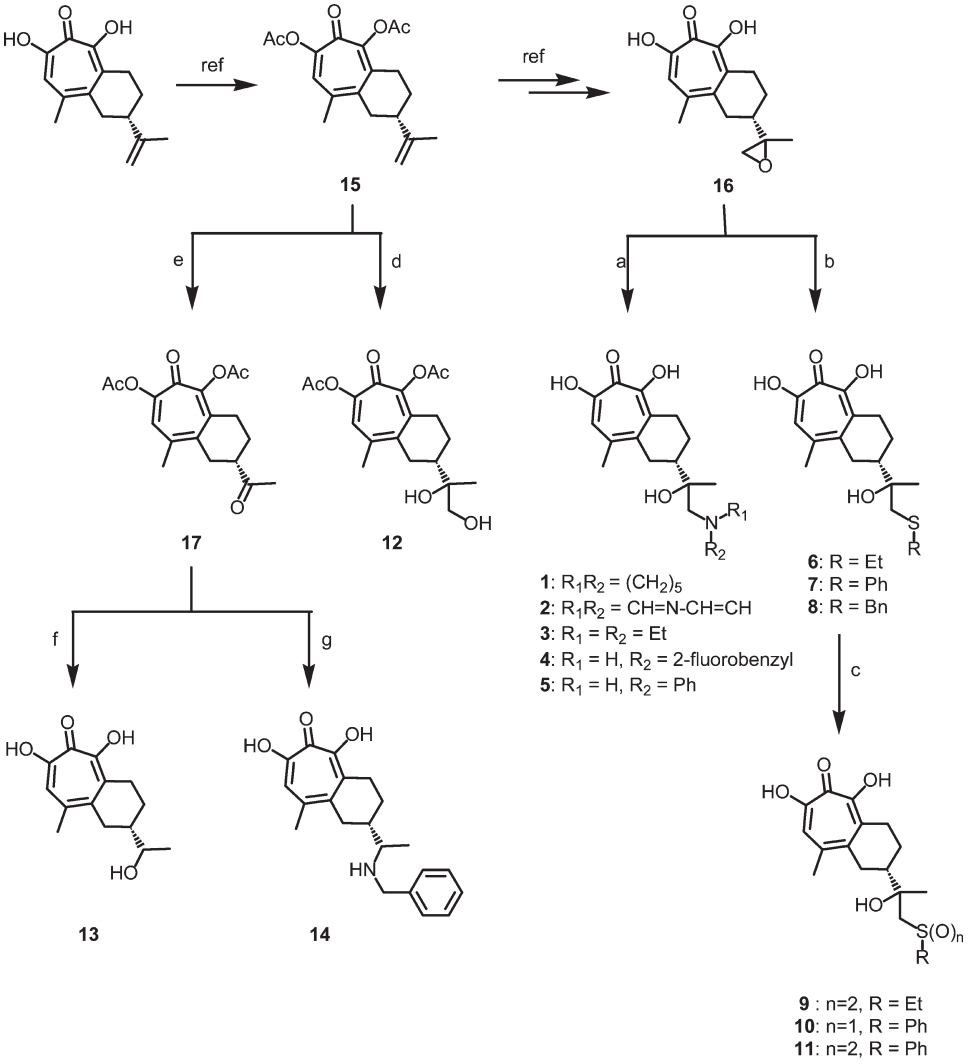

[a] Reagents and conditions: (a) NHR_1R_2, $LiClO_4$, CH_3CN, 80 °C; (b) (i) PhSH, Et_3N, THF, reflux, (ii) EtSH or BnSH, NaH, MeOH, rt; (c) *m*-CPBA, DCM; (d) OsO_4, *N*-methylmorpholine oxide, acetone/H_2O; (e) OsO_4, $NaIO_4$, $NaHCO_3$, *t*-BuOH/H_2O; (f) $NaBH_4$, MeOH, reflux; (g) $BnNH_2$, $NaBH(OAc)_3$, 1,2-dichloroethane.

RNA/DNA hybrid is illustrated in Figure 4a and quantification of cleavage data in Figure 4b. In this experiment, compounds **1**−**14** were assayed at a final concentration of 20 μM.

In all instances, primary RNase H-mediated hydrolysis occurred at the 5′-pG< >pA-3′ PPT/U3 junction, with additional cleavage at the immediately adjacent 5′-pG-pG-3′ sequences. Thus, while differing levels of inhibition were observed with compounds **1**−**14**, none altered cleavage specificity in the PPT assay. In keeping with the data of Table 2, compound **9** was almost 100% effective in inhibiting PPT/U3 cleavage, while compounds **2**, **4**, **10**, and **14** were poorly active. Interestingly, some inhibitors, e.g. compounds **3** and **11**, were ineffective in inhibiting PPT/U3 cleavage while more active on the nonspecific RNA/DNA hybrid. In contrast, compound **5** was more active in blocking PPT/U3 cleavage than inhibiting polymerase-independent cleavage on the nonspecific substrate. Data of Table 2 and Figure 3 thus illustrate potential benefits of including model systems that mimic some of the more complex RNase H-mediated events in HIV replication as screening tools.

Inhibition of DNA Polymerase Activity by Manicol Analogues. Although our crystallographic data indicated a single manicol binding site in the RNase H domain, Didierjean et al.[7] have demonstrated that dihydroxytropolones can inhibit both the DNA polymerase and RNase H functions of HIV-1 RT. In addition, Su et al. recently presented crystallographic evidence that a naphthyridinone-based inhibitor, indentified through their RNase H screening efforts, bound close to the NNRTI binding site of the DNA polymerase domain in a metal-independent manner.[18] Such "action from a distance" is not unexpected because similar observations have been reported with both NNRTIs[32] and a dihydroxybenzoyl-naphthyl hydrazone-based inhibitor.[16] To examine the specificity of our manicol analogues, we therefore determined their effect on the DNA polymerase activity of wild type p66/p51 HIV-1 RT and RNase H-deficient derivatives, $p66^{EQ}$/p51 and $p66^{DA}$/p51, which harbor mutations in one of the catalytically essential amino acids contacted by manicol (E478 and D549, respectively, Figure 3) that would be predicted to interfere with α-hydroxytropolone binding. Inhibition

dx.doi.org/10.1021/jm2000757 |*J. Med. Chem.* 2011, 54, 4462–4473

Table 2. Inhibition of HIV-1 RNase H Enzymatic Activity and the Cytopathic Effect of α-Hydroxytropolones on HIV-1_{RF} Virus Replication on CEM-SS Cells

	in vitro	viral replication	
inhibitor	IC_{50} (μM)	EC_{50} (μM)	CC_{50} (μM)
β-thujaplicinol	0.21[a]	np[b]	2.3
manicol	0.60[a]	np	13.6
1	0.82 ± 0.08	10.2	>50
2	1.9 ± 0.4	42.1	>50
3	0.50 ± 0.07	<50%[c]	>50
4	1.2 ± 0.1	np	>50
5	1.2 ± 0.2	7.4	31.7
6	0.38 ± 0.07	<50%	25.8
7	0.93 ± 0.10	11.5	17.8
8	1.3 ± 0.2	4.2	17.4
9	0.24 ± 0.02	<50%	10.4
10	1.3 ± 0.2	14.5	>50
11	0.51 ± 0.10	21.2	>50
12	1.9 ± 0.2	np	>50
13	0.68 ± 0.03	6.9	26.1
14	0.96 ± 0.07	10.6	16.7

[a] Reference 14. [b] np = no protective effect on cytopathicity of virus. [c] <50% = protective effect less than 50% of control, i.e. weak activity.

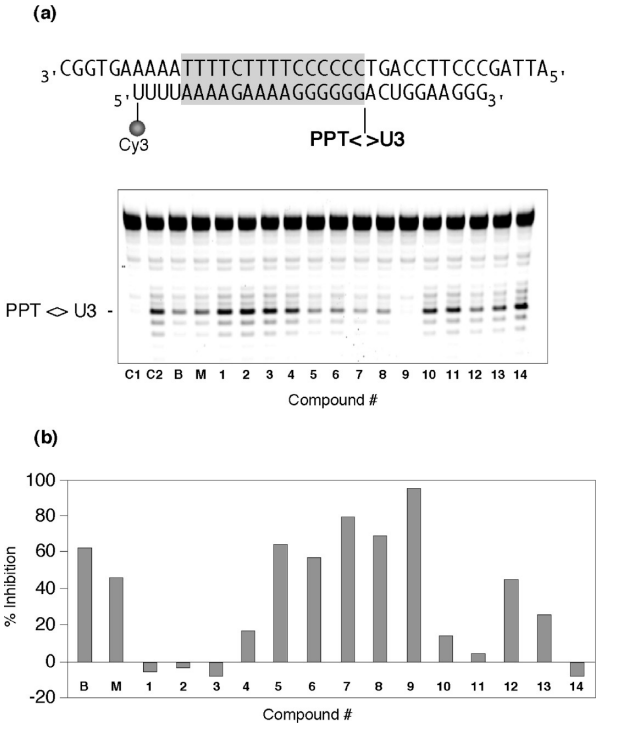

Figure 4. α-Hydroxytropolone inhibition of RNase H-mediated release of the HIV-1 PPT primer from (+) RNA. (a) Upper, schematic model of RNA/DNA substrate, indicating the RNase H cleavage site at the PPT/U3 junction (< >). The PPT is indicated by the shaded box. Lower, PPT cleavage assay. Lane **C1**, no enzyme; Lane **C2**, no inhibitor; lane **B**, β-thujaplicinol; lane **M**, manicol. The PPT/U3 cleavage product is indicated. (b) Quantification of PPT cleavage data. All inhibitors were evaluated at 20 mM.

of DNA polymerase activity of RNase H-deficient enzymes would be diagnostic of a second binding mode within, or proximal to, the DNA polymerase active site, possibly resulting from more extensive modification of manicol.

The results of our analysis are presented in Figure 5. In general, manicol analogues had minimal effect on DNA polymerase activity of RNase H-deficient $p66^{EQ}$/p51 and $p66^{DA}$/p51 RT, suggesting specificity for the RNase H active site. However, two exceptions were noted, namely compounds **5** and **10**, which significantly and consistently inhibited DNA-dependent DNA polymerase activity of both mutants. Although crystallographic evidence is presently unavailable, compounds **5** and **10** thus appear capable of occupying a second site on HIV-1 RT.

Antiviral Activity of Manicol Analogues. The parent compounds β-thujaplicinol and manicol showed no protection against the cytopathic effect of HIV, with CC_{50} values of 2.3 and 13.6 μM (Table 2), consistent with previous reports from our laboratory. Compounds **4** and **12** also showed no protection against virus cytopathicity but were not cytotoxic up to a concentration of 50 μM. Compounds **3**, **6**, and **9** showed slight protection against cytopathicity. However in each case, the protection did not reach 50% of control cell growth, and these compounds were therefore judged inactive.

Compounds **1**, **2**, **5**, **7**, **8**, **10**, **11**, **13**, and **14** all showed protection against the cytopathicity of the virus, with EC_{50} values ranging from 4.2 μM (compound **8**) to 42.1 μM (compound **2**). In vitro therapeutic indices (CC_{50}/EC_{50}) were quite modest, ranging from 1.2 to 4.9 (compound **1**). It was encouraging, however, that the cytotoxicity of all of the active compounds was reduced compared to their manicol precursor.

Modeling Compounds 14 and 9 into the RNase H Active Site. To gain insight into how manicol modification affects inhibitor binding, we performed energy minimization experiments on model RNase H−inhibitor complexes in which compound **14** and **9** were substituted for manicol. These derivatives were selected for modeling to determine whether their distinctive amine or sulfide constituents, respectively, would be predicted to form hydrogen bonds, or other stabilizing interactions, with RNase H residues, particularly His539. Models were constructed using coordinates from the RT−manicol cocrystal structure reported herein as described in the Experimental Section and were subjected to two rounds of energy minimization.

As illustrated in Figure 6A, the amino group of compound **14** is several angstroms from the His539 side chain and oriented toward solvent rather than the imidazole ring. This may reflect electrostatic repulsion between charged or partially charged nitrogen atoms within the two groups or because interaction between the phenyl substituent of compound **14** and the His539 imidazole ring is more favorable. Modeling of compound **9** (Figure 6B) suggests that both sulfonyl oxygens are located within hydrogen bonding distance of His539 Nδ. Moreover, because the partial charges of the sulfonyl oxygens and the δ-nitrogen are predicted to be opposed, electrostatic interaction between these two groups may serve to stabilize the enzyme−inhibitor complex. In the cases of these two compounds, different chemical moieties appear to mediate their interaction with His539. Nevertheless, both models of Figure 6 suggest that IC_{50} differences among manicol derivatives most likely reflect changes in their interaction with the side chain of this conserved residue and that stabilizing this interaction is the key to improving these inhibitors.

dx.doi.org/10.1021/jm2000757 |J. Med. Chem. 2011, 54, 4462–4473

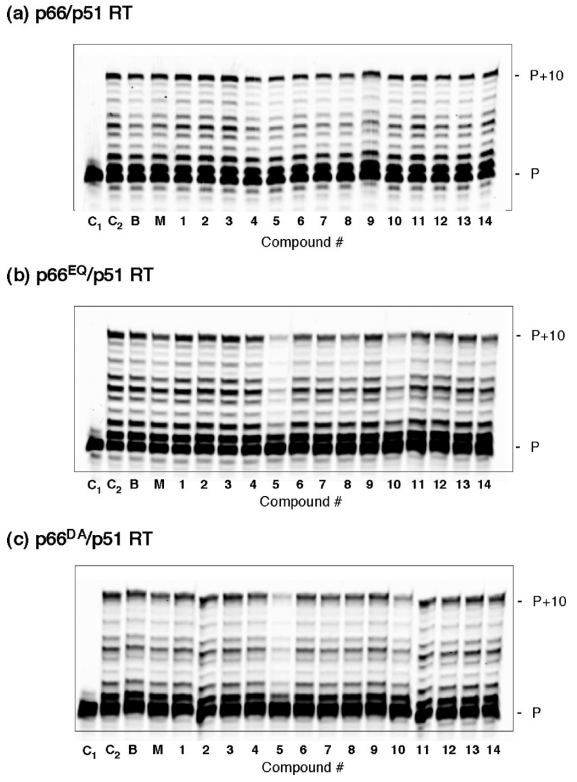

Figure 5. Influence of RNase H inhibitors on the DNA-dependent DNA polymerase activity of HIV-1 RT. (a), wild type enzyme; (b), RNase H mutant p66^{E478Q}/p51; (c), RNase H mutant p66^{D549A}/p51. Lane notation is as in the legend to Figure 3. All inhibitors were tested at 20 μM. **P**, unextended primer; **P+10**, fully extended primer.

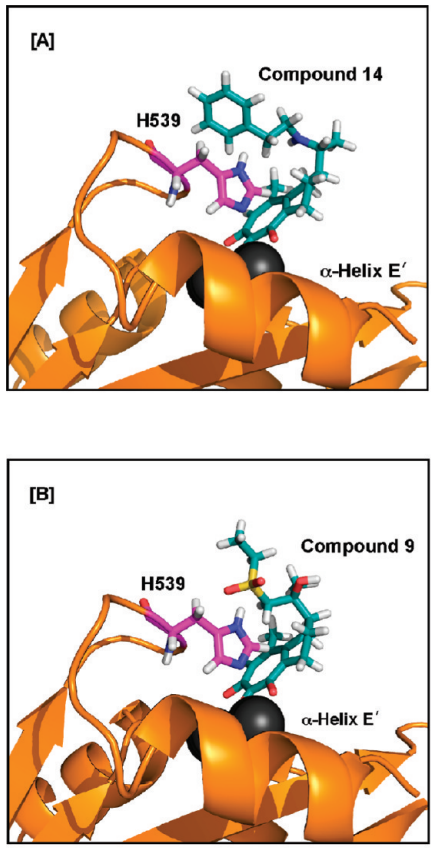

Figure 6. Modeling of compound **14** [A] and **9** [B] into the RNase H active site of HIV-1 RT. For convenience, only the RNase H active site is illustrated. The Mn^{2+} cations are represented as as dark-gray spheres. Atoms of residue H539 and compounds **14** and **9** are shown as sticks and colored as follows: carbon (H539) = cyan; carbon (compound **14** and **9**) = purple; nitrogen = blue; oxygen = red; sulfur = yellow; hydrogen = white.

DISCUSSION AND CONCLUSIONS

Successful combination antiretroviral therapy will require continued efforts to develop a variety of small molecule antagonists that interact synergistically at different sites of their target molecule. For HIV-1 RT, this has been exemplified by NRTI/NNRTI combinations targeting the DNA polymerase active site and a hydrophobic pocket at the base of the p66 thumb, respectively. With regard to RNase H function, Su et al. have recently published the structure of HIV-1 RT containing nevirapine in the NNRTI binding pocket and a naphthyridinone-containing inhibitor at the RNase H active site. In the present study, we present a complementary high-resolution structure of RT containing the second-generation diarylpyrimidine derivative **18** in the NNRTI binding site and manicol at the RNase H active site. Moreover, we show that manicol derivatives retain in vitro potency and also inhibit HIV-1 replication, albeit with low therapeutic indices. Because the structure of RNase H active site is relatively flat and open, allowing a large substrate to be accommodated, an important consideration is to design inhibitors that interact with active site residues and coordinate divalent metal ions in order to improve potency and selectivity. His539 is clearly an attractive target based on its important role in catalysis and the fact that it can interact with other aromatic residues as well as be hydrogen-bonded with positive or negative charged molecules. Our cocrystal structure shows how manicol could achieve favorable interactions with His539 yet maintain its ability to coordinate divalent metal ions. Modeling studies of Figure 6 also indicate that a number of additional interactions with His539 could be achieved by introducing sulfonyl or aromatic groups into manicol. In addition, adding bulky substituents to manicol might be beneficial by reducing cellular toxicity via decreasing binding affinity for other cellular metalloenzymes, which may explain enhanced antiviral activity in cell culture we observed here. Thus, while clinical evaluation of α-hydroxytropolones is premature, our work provides an important platform for structure-based drug design as well as in vivo studies to better characterize their mode of action.

Despite our structural and biochemical studies, it remains to be established that RNase H is the in vivo target of our novel α-hydroxytropolones. Inhibition of RNase H activity predicts that virus replication would be interrupted at the step of (−) strand DNA transfer, where nascent DNA relocates to the 3′ end of the viral genome via homology between the 5′ and 3′ repeat (R) regions of the (+) viral genome.[33] Successful strand transfer requires RNase H-mediated cleavage of the RNA/DNA replication intermediate to allow the newly synthesized (−) strand DNA to dissociate from the donor and access the acceptor template. Accumulation of (−) strong-stop DNA would thus indicate loss in RNase H function. An alternative strategy would be the isolation of RNase H inhibitor-resistant mutants and

dx.doi.org/10.1021/jm2000757 |J. Med. Chem. 2011, 54, 4462–4473

localization of the inactivating lesion to the RNase H domain. Although the therapeutic indices determined here are low, they should be sufficient to allow such in vivo manipulations.

Another issue that can be addressed is the "dynamic copy choice" model of Nikolenko et al.,[34] who have proposed that perturbing the balance between the DNA polymerase and RNase H activities may promote dissociation of the replication complex and interrupt virus replication. By introducing mutations into the RNase H domain which inhibit hydrolysis, these authors demonstrated increased NRTI resistance, inferring that increased residency at the DNA polymerase catalytic center provides more time for excision of the chain terminating NRTI. One implication of this model would be that RNase H inhibitors could not be used in combination with AZT in a clinical setting. Rather than employ mutant enzymes that may have subtle effects on both catalytic activities, AZT sensitivity can now be assessed in vivo in the presence of an RNase H inhibitor. In the event that an NRTI/RNase H inhibitor combination proves deleterious, studies of Shaw-Reid et al.[35] and Budihas et al.[6] have shown that NNRTIs are synergistic with both diketo acid- or α-hydroxytropolone-based RNase H inhibitors, suggesting that regimens including NNRTI and RNase H inhibitors might have therapeutic benefits.

Finally, in a manner analogous to the NRTI/NNRTI combinations, the possibility of allosteric and active site RNase H inhibitors is worth considering. Recently, we reported a structure−activity relationship of several vinylogous ureas that inhibit HIV-1 RNase H activity in the sub- to low-micromolar range.[13] Protein footprinting,[12] molecular modeling,[13] and in vitro site-directed mutagenesis (Chung, S. et al., unpublished results) collectively implicate the p51 thumb as the vinylogous urea binding site, suggesting they function by altering RT subunit or subdomain geometry. As mentioned earlier, our crystallographic analysis indicates that manicol makes multiple contacts with the highly conserved His539 of the flexible "His loop". At the same time, modeling studies of Chung et al.[13] indicate that the vinylogous urea binding site is also in the vicinity of His539. Conceivably, a bidentate inhibitor comprising these two structural classes may combine the properties of both to provide improved selectivity.

EXPERIMENTAL SECTION

General. All air or moisture sensitive reactions were performed under positive pressure of nitrogen with oven-dried glassware. Anhydrous solvents such as tetrahydrofuran (THF), toluene, dichloromethane, *N*,*N*-dimethylformamide (DMF), acetonitrile, methanol, and triethylamine were purchased from Sigma-Aldrich. Purifications of the compounds were performed on Waters UPLC or Biotage SP systems. Samples were analyzed for purity on an Agilent 1200 series LC/MS equipped with a Zorbax Eclipse XDB-C18 reverse phase (5 μm, 4.6 mm × 150 mm) column having a flow rate of 0.8 mL/min. The mobile phase was a mixture of acetonitrile and H_2O each containing 0.05% trifluoroacetic acid. Gradient of 4−100% acetonitrile (0.05% TFA) over 7 min with flow rate of 0.8 mL/min using Luna C18 3 μm 3 mm × 75 mm column. All of the analogues for assay have purity greater than 95%. High resolution mass spectrometry was recorded on Agilent 6210 time-of-flight LC/MS system. Note: all of the final analogues are the mixture of diastereomers which are inseparable on preparative HPLC. Purified oligonucleotides for the fluorescence-based RNase H were purchased from TriLink Biotechnologies (San Diego, CA). His-p66/His-p51 HIV-1 RT, derived from the HIV-1_{HXB2} isolate,[36] was expressed and purified as previously reported. This enzyme is identical in sequence with respect to the residues discussed in modeling studies.

5,7-Dihydroxy-2-(1-hydroxy-1-methyl-2-piperidin-1-yl-ethyl)-9-methyl-1,2,3,4-tetrahydro Benzocyclohepten-6-one (1). To a solution of manicol epoxide (**16**) (7 mg, 0.027 mmol) in acetonitrile (0.5 mL) was added piperidine (18.2 mg, 0.213 mmol, 8.0 equiv) and lithium perchlorate (5.7 mg, 0.053 mmol, 2 equiv). The mixture was refluxed for 1 h. After cooling to room temperature, another 1.5 mL of acetonitrile was added and the mixture was directly subject to preparative HPLC purification to give the desired product **1** as a brownish solid (4 mg, 54%). ^{1}H NMR (400 MHz, DMSO-d_6) δ 8.83−8.58 (br s, 1H), 7.37 (s, 1H), 5.75 (s, 1H), 5.55−5.23 (br s, 1H), 3.62−3.40 (m, 2H), 3.29−3.17 (m, 2H), 3.13−2.96 (m, 3H), 2.92−2.67 (m, 2H), 2.59−2.50 (m, 3H), 2.41 (s, 3H), 2.05−1.85 (m, 1H), 1.85−1.68 (m, 4H), 1.67−1.57 (m, 1H), 1.52−1.37 (m, 1H), 1.29 and 1.25 (s, 3H). LC/MS: retention time, 3.449 min. HRMS: *m*/*z* (M + H$^+$) = 348.2176 (calcd for $C_{20}H_{30}NO_4S$ = 348.2175).

5,7-Dihydroxy-2-(1-hydroxy-2-imadazol-1-yl-1-methyl−ethyl)-9-methyl-1,2,3,4-tetrahydro Benzocyclohepten-6-one (2) was prepared in the same manner as **1** except by using imidazole as a nucleophile. ^{1}H NMR (400 MHz, DMSO-d_6) δ 9.03 and 9.01 (s, 1H), 7.72−7.64 (m, 2H), 7.38 and 7.36 (s, 1H), 5.25−5.03 (br s, 1H), 4.36−4.21 (m, 2H), 3.80−3.30 (br s, 2H), 3.20−3.00 (m, 1H), 3.00−2.60 (m, 2H), 2.44 and 2.40 (s, 3H), 2.62−2.47 (m, 1H), 2.25−1.92 (m, 1H), 1.75−1.48 (m, 1H), 1.45−1.25 (m, 1H), 1.01 and 1.00 (s, 3H). LC/MS: retention time, 3.337 min. HRMS: *m*/*z* (M + H$^+$) = 331.1651 (calcd for $C_{18}H_{23}N_2O_4$ = 331.1658).

2-(2-Diethylamino-1-hydroxy-1-methyl-ethyl)-5,7-dihydroxy-9-methyl-1,2,3,4-tetrahydrobenzocyclohepten-6-one (3) was prepared in the same manner as **1** except by using diethylamine as a nucleophile. ^{1}H NMR (400 MHz, DMSO-d_6) δ 8.56−8.33 (br s, 2H), 7.38 and 7.37 (s, 1H), 5.50−5.28 (br s, 1H), 3.95−3.35 (m, 4H), 3.34−3.10 (m, 4H), 3.10−2.90 (m, 1H), 2.87−2.55 (m, 1H), 2.54 and 2.52 (s, 3H), 2.25−1.85 (m, 1H), 1.75−1.58 (m, 1H), 1.35−1.15 (m, 10H). LC/MS: retention time, 3.427 min. HRMS: *m*/*z* (M + H$^+$) = 336.2171 (calcd for $C_{19}H_{30}NO_4$ = 336.2175).

2-[2-(2-Fluoro-benzylamino)-1-hydroxy-1-methyl-ethyl]-5,7-dihydroxy-9-methyl-1,2,3,4-tetrahydrobenzocyclohepten-6-one (4) was prepared in the same manner as **1** except by using 2-fluoroaniline as a nucleophile. ^{1}H NMR (400 MHz, DMSO-d_6) δ 8.90−8.60 (br s, 2H), 7.70−7.61 (m, 1H), 7.54−7.45 (m, 1H), 7.36 and 7.35 (s, 1H), 7.34−7.35 (m, 2H), 5.48−5.15 (br s, 1H), 4.25 (s, 2H), 3.20−2.90 (m, 3H), 2.90−2.61 (m, 2H), 2.38 and 2.34 (s, 3H), 2.50−2.35 (m, 2H), 2.15−1.92 (m, 1H), 1.80−1.65 (m, 1H), 1.33−1.13 (m, 1H), 1.20 and 1.18 (s, 3H). LC/MS: retention time, 3.844 min. HRMS: *m*/*z* (M + H$^+$) = 388.1914 (calcd for $C_{22}H_{27}FNO_4$ = 388.1924).

5,7-Dihydroxy-2-(1-hydroxy-1-methyl-2-phenylamino-ethyl)-9-methyl-1,2,3,4-tetrahydrobenzocyclohepten-6-one (5) was prepared in the same manner as **1** except by using aniline as a nucleophile. ^{1}H NMR (400 MHz, $CDCl_3$) δ 7.50 and 7.49 (s, 1H), 7.34−7.25 (m, 2H), 7.05−6.94 (m, 3H), 3.43−3.17 (m, 2H), 3.04−2.82 (m, 2H), 2.64−2.33 (m, 2H), 2.48 and 2.46 (s, 3H), 2.23−2.03 (m, 1H), 2.02−1.84 (m, 2H), 1.53−1.39 (m, 1H), 1.38 and 1.31 (s, 3H). LC/MS: retention time min, 4.715 min. HRMS: *m*/*z* (M + H$^+$) = 356.1864 (calcd for $C_{21}H_{26}NO_4$ = 356.1862).

2-(2-Ethylsulfanyl-1-hydroxy-1-methyl-ethyl)-5,7-dihydroxy-9-methyl-1,2,3,4-tetrahydrobenzocyclohepten-6-one (6). was prepared in the same manner as **5** except by using ethanethiol as a nucleophile. ^{1}H NMR (400 MHz, $CDCl_3$) δ 7.49 and 7.48 (s, 1H), 3.28−3.24 and 3.24−3.19 (m, 1H), 3.03−2.78 (m, 2H), 2.76−2.64 (m, 2H), 2.60−2.50 (m, 1H), 2.48 and 2.47 (s, 3H), 2.16−2.02 (m, 2H), 1.83−1.71 (m, 1H), 1.70−1.59 (m, 1H), 1.56−1.25 (m, 4H), 1.40 and 1.38 (s, 3H). LC/MS: retention time, 5.529 min. HRMS: *m*/*z* (M + H$^+$) = 325.1466 (calcd for $C_{17}H_{25}O_4S$ = 325.1474).

5,7-Dihydroxy-2-(1-hydroxy-1-methyl-2-phenylsulfanyl-ethyl)-9-methyl-1,2,3,4-tetrahydrobenzocyclohepten-6-one (7). To a solution of **16** (15 mg, 0.057 mmol) in THF (1 mL) was added thiophenol (0.20 mL, 1.94 mmol, 34 equiv) and Et_3N (0.08 mL, 0.57 mmol, 10 equiv), and the solution was refluxed overnight. After cooling to room temperature, the mixture was directly purified by HPLC to give the desired product **7** as a light-yellow solid (10 mg, 47%). ^{1}H NMR (400 MHz, $CDCl_3$) δ 7.50 and 7.49 (s, 1H), 7.46−7.39 (m, 2H), 7.33−7.18 (m, 3H), 3.37−3.10 (m, 3H), 3.05−2.91 (m, 1H), 2.91−2.76 (m, 1H), 2.67−2.50 (m, 2H), 2.48 and 2.42 (s, 3H), 1.98−1.85 (m, 1H), 1.49−1.33 (m, 1H), 1.32 and 1.26 (s, 3H). LC/MS: retention time, 6.101 min. HRMS: m/z (M + H^+) = 373.1472 (calcd for $C_{21}H_{25}O_4S$ = 373.1474).

2-(2-Benzylsulfanyl-1-hydroxy-1-methyl-ethyl)-5,7-dihydroxy-9-methyl-1,2,3,4-tetrahydrobenzocyclohepten-6-one (8). To a solution of BnSH (26 mg, 0.21 mmol) in MeOH (1 mL) was added NaH (4.6 mg, 0.19 mmol), and the mixture was stirred for 10 min. **16** (5 mg, 0.019 mmol) was added, and the mixture was stirred overnight at room temperature and directly purified by preparative HPLC to give the desired product **8** (3 mg, 58%). ^{1}H NMR (400 MHz, DMSO-d_6) δ 7.35 and 7.34 (s, 1H), 7.33−7.28 (m, 4H), 7.25−7.20 (m, 1H), 3.79−3.76 (m, 2H), 3.06−2.94 (m, 1H), 2.82−2.60 (m, 5H), 2.48−2.36 (m, 1H), 2.34 and 2.33 (s, 3H), 1.30−1.16 (m, 2H), 1.15 and 1.13 (s, 3H). Retention time: 6.157 min. HRMS: m/z (M + H^+) = 387.1620 (calcd for $C_{22}H_{27}O_4S$ = 387.1630).

2-(2-Ethanesulfonyl-1-hydroxy-1-methyl-ethyl)-5,7-dihydroxy-9-methyl-1,2,3,4-tetrahydrobenzocyclohepten-6-one (9) was prepared through oxidation of corresponding sulfide **6** with *m*-CPBA in CH_2Cl_2 at room temperature. ^{1}H NMR (400 MHz, DMSO-d_6) δ 7.36 and 7.35 (s, 1H), 3.42−3.26 (m, 2H), 3.11−2.98 (m, 1H), 2.89−2.67 (m, 2H), 2.60−2.45 (m, 4H), 2.40 and 2.39 (s, 3H), 2.02−1.79 (m, 1H), 1.77−1.65 (m, 1H), 1.45−1.12 (m, 3H), 1.07 and 1.05 (s, 3H). LC/MS: retention time, 4.323. HRMS: m/z (M + H^+) = 357.1370 (calcd for $C_{17}H_{25}O_6S$ = 357.1372).

2-(2-Benzylsulfanyl-1-hydroxy-1-methyl-ethyl)-5,7-dihydroxy-9-methyl-1,2,3,4-tetrahydrobenzocyclohepten-6-one (10) was prepared by oxidation of corresponding sulfide with *m*-CPBA at −78 °C, while 2-(2-benzenesulfinyl-1-hydroxy-1-methyl−ethyl)-5,7-dihydroxy-9-methyl-1,2,3,4-tetrahydrobenzocyclohepten-6-one (**11**) was prepared by oxidation using *m*-CPBA at room temperature. **10**: ^{1}H NMR (400 MHz, DMSO-d_6) δ 7.72−7.66 (m, 2H), 7.63−7.52 (m, 3H), 7.37 and 7.36 (s, 1H), 3.23−2.80 (m, 4H), 2.62−2.50 (m, 2H), 2.42 and 2.41 (s, 3H), 2.15−1.90 (m, 3H), 1.40−1.15 (m, 4H). LC/MS: retention time, 4.767 min. HRMS: m/z (M + H^+) = 389.1422 (calcd for $C_{21}H_{25}O_5S$ = 389.1423). **11**: ^{1}H NMR (400 MHz, DMSO-d_6) δ 10.61 (s, 1H), 9.98 (s, 1H), 7.96−7.87 (m, 2H), 7.74−7.66 (m, 1H), 7.75−7.58 (m, 1H), 7.45−7.38 (m, 2H), 4.10−3.50 (m, 3H), 2.64−2.54 (m, 2H), 2.53 and 2.52 (s, 3H), 2.34−2.18 (m, 2H), 2.17−1.94 (m, 1H), 1.94−1.76 (m, 1H), 1.43−1.28 (m, 1H), 1.24 and 1.23 (s, 3H). LC/MS: retention time, 5.123 min. HRMS: m/z (M + H^+) = 405.1354 (calcd for $C_{21}H_{25}O_6S$ = 405.1360).

2-(1,2-Dihydroxy-1-methyl-ethyl)-5,7-dihydroxy-9-methyl-1,2,3,4-tetrahydrobenzocyclohepten-6-one (12). To a solution of diacetate **15** (5 mg, 0.014 mmol) in acetone/H_2O (0.19 mL/0.02 mL) was added 2.5 wt % *tert*-BuOH OsO_4 solution (7.7 μL, 0.757 μmol) and *N*-methylmorpholine oxide (3.4 mg, 0.029 mmol), and the mixture was stirred for 3 h. EtOAc (10 mL) was added, and the solution was washed with 10% aqueous Na_2SO_3 solution and brine. The organic layer was dried over $MgSO_4$. After the removal of EtOAc, the crude product was redissolved in MeOH (2 mL) and then refluxed for 5 h. The solution was concentrated to 2 mL and directly subject to preparative HPLC purification to give the desired diol **12** (3 mg, 71%). ^{1}H NMR (400 MHz, DMSO-d_6) δ 7.36 and 7.35 (s, 1H), 3.42−3.27 (m, 2H), 3.11−2.97 (m, 1H), 2.89−2.65 (m, 2H), 2.58−2.44 (m, 1H), 2.39 and 2.38 (s, 3H), 2.00−1.81 (m, 1H), 1.76−1.64 (m, 1H), 1.36−1.20 (m, 2H), 1.06 and 1.05 (s, 3H). LC/MS: retention time, 3.795 min. HRMS: m/z (M + H^+) = 281.1386 (calcd for $C_{15}H_{21}O_5$ = 281.1389).

5,7-Dihydroxy-2-(1-hydroxy-ethyl)-9-methyl-1,2,3,4-tetrahydrobenzocyclohepten-6-one (13). To a solution of **15** (22 mg, 0.07 mmol) in *tert*-BuOH/H_2O (1.8 mL/0.36 mL) was added 2.5 wt % *tert*-BuOH OsO_4 solution (0.42 mL, 0.042 mmol), $NaIO_4$ (123 mg, 0.58 mmol), and $NaHCO_3$ (81 mg, 0.96 mmol), and the mixture was stirred 2 h at room temperature. 10% Na_2SO_3 (1.5 mL) was added, and the mixture was stirred for 0.5 h and extracted with CH_2Cl_2 (3 × 10 mL), and the combined organic layers were washed with brine and dried over Na_2SO_4. After the removal of organic solvent, the residue was purified by column chromatography (EtOAc/hexane 1/1) to give the desired ketone **17** (20 mg, 90%). **17** was then dissolved in MeOH (2 mL), and $NaBH_4$ (6 mg, 0.16 mmol) was added and stirred at room temperature for 0.5 h. After the complete reduction of the ketone monitored by LC/MS, the mixture was further refluxed for 5 h and directly purified by preparative HPLC to give **13**. ^{1}H NMR (400 MHz, $CDCl_3$) δ 7.51 and 7.50 (s, 1H), 3.84−3.77 and 3.76−3.63 (m, 1H), 3.29−3.18 (m, 1H), 3.05−2.94 (m, 2H), 2.84 and 2.79 (d, J = 3.9 Hz, 1H), 2.70−2.51 (m, 1H), 2.51 and 2.48 (s, 3H), 2.16−2.06 and 2.03−1.93 (m, 1H), 1.78−1.66 (m, 1H), 1.49−1.34 (m, 1H), 1.31 (d, J = 6.3 Hz, 3H). LC/MS: retention time, 4.315 min. HRMS: m/z (M + H^+) = 251.1280 (calcd for $C_{14}H_{19}O_4$ = 251.1283).

2-(1-Benzylamino-ethyl)-5,7-dihydroxy-9-methyl-1,2,3,4-tetrahydrobenzocyclohepten-6-one (14). To a solution of **17** (5 mg, 0.015 mmol) in 1,2-dichloroethane (0.1 mL) was added benzylamine (1.6 μL, 0.016 mmol) and sodium triacetoxyborohydride (4.5 mg, 0.021 mmol), and the mixture was stirred overnight at room temperature. LC/MS indicated the formation of deacetylated product **14**. The mixture was directly purified by preparative HPLC to give desired product **14** (3 mg, 59%). ^{1}H NMR (400 MHz, DMSO-d_6) δ 9.03−8.85 (br s, 1H), 8.73−8.56 (br s, 1H), 7.63−7.51 (m, 2H), 7.51−7.40 (m, 3H), 7.37 (s, 1H), 4.37−4.14 (m, 2H), 3.45−3.27 (m, 1H), 3.20−3.00 (m, 1H), 2.97−2.63 (m, 2H), 2.58−2.44 (m, 2H), 2.39 and 2.37 (s, 3H), 2.25−2.05 (m, 1H), 2.03−1.93 and 1.92−1.83 (m, 1H), 1.42−1.28 (m, 4H). LC/MS: retention time, 3.913 min. HRMS: m/z (M + H^+) = 340.1908 (calcd for $C_{21}H_{26}NO_3$ = 340.1913).

HIV-1 RT Expression and Purification for Biochemical Analysis. $(His)_6$-tagged p66/p51 HIV-1_{HXB2} RT and the RNase H-deficient mutants were expressed from recombinant *Escherichia coli* and purified by a combination of immobilized metal affinity and ion exchange chromatography as previously described.[37] Purified enzymes were stored at −20 °C in a buffer of 50 mM Tris/HCl, pH 7.0, 25 mM NaCl, 1 mM EDTA, 1 mM dithiothereitol, and 50% (v/v) glycerol.

RNase H Inhibitor Analysis. IC_{50} values were determined as previously reported,[6] using an 18-nucleotide 3′-fluourescein-labeled RNA annealed to a complementary 18-nucleotide 5′-dabsyl-labeled DNA. Cleavage of the HIV-1 polypurine tract (PPT) primer was performed with a 29 nt Cy5-labeled RNA (5′-Cy5-*UUU UAA AAG AAA AGG GGG G*AC UGG AAG GG*-3′, where *represents the PPT 3′ terminus) hybridized to a 40 nt DNA (5′-ATT AGC CCT TCC AGT CCC CCC TTT TCT TTT AAA AAG TGG C-3′). The reaction was initiated by adding 1 μL of 100 mM $MgCl_2$ to 9 μL of mixture containing 4 ng of enzyme, 200 nM substrate, 20 μM α-hydroxytropolones in 50 mM Tris, pH 8.0, 80 mM KCl, 2 mM DTT, and 10% DMSO at 37 °C and quenched with 10 μL of a gel-loading buffer after 10 min. Hydrolysis products were fractionated by denaturing polyacrylamide gel electrophoresis and visualized by fluorescent imaging (Typhoon Trio+, GE Healthcare).

DNA Polymerase Assay. DNA-dependent DNA synthesis was measured on a fluorescently labeled duplex DNA prepared by annealing a 33-nt template, 5′-CAC TGC TCA AGA AGT TCC AAT CCT AAA

TAC ATA-3′, to the 5′-Cy5 -labeled primer 5′-ATG TAT GGG TAT GTA TTT AGG-3′. Polymerization was initiated by adding 1 μL of 2 mM dNTPs to 9 μL of mixture containing 4 ng of enzyme, 200 nM substrate, 20 μM α-hydroxytropolones in 10 mM Tris, pH 7.8, 80 mM KCl, 1 mM DTT, 10 mM $MgCl_2$, and 10% DMSO at 37 °C. DNA synthesis was quenched with 10 μL of a gel-loading buffer after 10 min, and reaction products were analyzed by denaturing polyacrylamide gel electrophoresis and fluorescent imaging.

HIV-1 Cytopathicity Assay. This assay was conducted as previously reported.[38] Samples were dissolved in DMSO at 10 mM and diluted to a final high concentration of 50 μM in the 96-well assay plate, with 2-fold dilutions made to a low concentration of 0.78 μM. All samples were tested in duplicate. The HIV-1 virus strain RF was used to infect CEM-SS cells. Compound cytotoxicity was measured in the same assay plate using uninfected cells. Regression analysis was used to estimate the effective concentration (EC_{50}) as well as the cytotoxic concentration (CC_{50}).

Expression and Purification of HIV-1 RT for Structural Studies. An HIV-1 RT variant designated RT52A was used for X-ray diffraction studies. In this variant, which was optimized for crystallization of RT with nucleoside or non-nucleoside RT inhibitors (NRTIs and NNRTIs, respectively), the p66 subunit was truncated at residue 555. The p51 subunit contained a HRV14 3C protease cleavable N-terminal hexahistidine tag and was truncated at residue 428. Both subunits contained the mutation C280S. The p66 subunit also contained the mutations K172A and K173A.[39] RT52A was expressed and purified as previously described.[39] Briefly, 1 mM IPTG was used to induce BL21-CodonPlus-RIL (Stratagene) containing a plasmid encoding both subunits of RT69A at an OD600 of 0.9 and the culture was incubated for three hours at 37 °C. The cells were pelleted and lysed by sonication. Protein was purified by Ni-NTA according to manufacturers' recommendations (Qiagen) with the following modifications: each buffer contained 600 mM NaCl, no lysozyme was added, and a 1.2 M NaCl wash was added. Eluted protein was incubated with HRV14 3C protease overnight at 4 °C. A Mono Q purification step was performed as described.[40] The protein was concentrated to 20 mg/mL in "RT storage buffer" (10 mM Tris pH 8.0, 75 mM NaCl) and stored at −80 °C.

Crystallization and Data Collection. HIV-1 RT52A was co-crystallized with manicol and **18** at 4 °C by vapor diffusion in micro-seeded hanging drops containing 1.2 μL each of 20 mg/mL protein (in a solution of 9.2 mM Tris pH 8.0, 68.7 mM NaCl, 3.6 mM manganese sulfate, 0.7 mM tris(2-carboxyethyl) phosphine (TCEP), 0.27% (w/v) β-ocytl glucopyranoside, 7% (v/v) DMSO, 0.9 mM manicol, and 0.7 mM **18**, preincubated for 30 min on ice) and a reservoir solution containing 50 mM HEPES pH 7.5, 100 mM ammonium sulfate, 15 mM manganese sulfate, 10 mM spermine, 5 mM TCEP, and 11% (w/w) PEG 8000. The chosen crystal was soaked for 120 s in a solution containing 50 mM HEPES pH 7.5, 50 mM NaCl, 100 mM ammonium sulfate, 15 mM manganese sulfate, 10 mM spermine, 15% (w/w) PEG 8000, 5% (w/w) PEG 400, 10% (v/v) DMSO, 11% (v/v) ethylene glycol, 6.5% (w/v) trimethylamine-*N*-oxide (TMAO), 0.69 mM manicol, and 0.34 mM **18**. The crystal was subsequently flash-cooled and stored in liquid N_2. X-ray data were collected at 100K and a wavelength of 1.1 Å at the National Synchrotron Light Source at Brookhaven National Laboratories, Beamline X25. The data were processed using the HKL-DENZO/SCALEPACK software suite.[41,42]

Structure Determination and Refinement. Phases for the diffraction data were determined by molecular replacement with the CCP4 program PHASER,[43] using an RT/**18** structure (PDB accession number 2ZD1)[44] as an initial search model. Stepwise model building and refinement were conducted using the "O" graphics package,[45] the Coot graphics package,[46] and CNS[47] with a bulk solvent correction (Table 1). Water molecules were built in both manually in Coot and using the program Refmac/ARP/wARP in the CCP4 software suite.[48−52] The geometry of the inhibitor and refinement of the RNH active site were improved by energy minimization using the Impact and PrimeX facilities of the Schrödinger software package (Schrödinger, LLC).

Molecular Modeling. A model of the HIV-1 RNase H domain in complex with an inhibitor and two Mn^{2+} cations was constructed from the HIV-1 RT-manicol cocrystal structure using Discovery Studio 2.0 (Accelrys, San Diego, CA). To create the starting structure for energy minimization, RT was truncated to include only the RNase H domain, the inhibitors were constructed directly from manicol using various "build" functions, and the CHARMm forcefield was applied to the entire structure via the "Simulation" tool. The modified structure was then subjected to two rounds of energy minimization (500 iterations each). Inhibitor atoms outside of the tropolone and cyclohexane rings, as well as the entire "His-loop" and side chains of α-helix E′, were permitted full flexibility according to the dictates of the minimization algorithm. The positions of other atoms were held fixed in order to minimize perturbation of the overall complex. Minimized structures were saved as PDB files and imported into PyMOL (Delano Scientific, LLC, San Francisco, CA) to generate the final image.

Accession Codes

PDB ID: 3QLJH.

AUTHOR INFORMATION

Corresponding Author

*Phone: 301-846-5256. Fax: 301-846-6013. E-mail: legrices@mail.nih.gov.

Author Contributions

⊥Contributed equally

ACKNOWLEDGMENT

S.C., J.R., J.B., J.W., and S.L.G. are supported by the Intramural Research Program of the National Cancer Institute, National Institutes of Health. J.J. and C.T. were supported by the Molecular Libraries Initiative of the National Institutes of Health Roadmap for Medical Research and the Intramural Research Program of the National Human Genome Research Institute. D. M.H. and E.A. were supported by NIH MERIT Award AI 27690.

ABBREVIATIONS USED

RNase, ribonuclease; HIV, human immunodeficiency virus; RT, reverse transcriptase; NNRTI, non-nucleoside RT inhibitor; NRTI, nucleoside RT inhibitor; AIDS, acquired immunodeficiency syndrome; HAART, highly active antiretroviral therapy; *m*-CPBA, *meta*-chloroperbenzoic acid; NMO, *N*-methyl morpholine oxide; PPT, Polypurine tract; AZT, azidothymidine; DMSO, dimethyl sulfoxide; THF, tetrahydrofuran; DMF, *N*,*N*-dimethyl formamide

REFERENCES

(1) Champoux, J. J. *Roles of Ribonuclease H in Reverse Transcription*; Cold Spring Harbor Laboratory Press: Cold Spring Harbor, NY, 1993; pp 103−118.

(2) Di Marzo Veronese, F.; Copeland, T. D.; DeVico, A. L.; Rahman, R.; Oroszlan, S.; Gallo, R. C.; Sarngadharan, M. G. Characterization of Highly Immunogenic p66/p51 as the Reverse Transcriptase of HTLV-III/LAV. *Science* **1986**, *231*, 1289–1291.

(3) Mous, J.; Heimer, E. P.; Le Grice, S. F. Processing protease and reverse transcriptase from human immunodeficiency virus type I polyprotein in Escherichia coli. *J. Virol.* **1988**, *62*, 1433–1436.

(4) Schatz, O.; Cromme, F. V.; Gruninger-Leitch, F.; Le Grice, S. F. Point mutations in conserved amino acid residues within the C-terminal domain of HIV-1 reverse transcriptase specifically repress RNase H function. *FEBS Lett.* **1989**, *257*, 311–314.

(5) Tisdale, M.; Schulze, T.; Larder, B. A.; Moelling, K. Mutations within the RNase H domain of human immunodeficiency virus type 1 reverse transcriptase abolish virus infectivity. *J. Gen. Virol.* **1991**, *72* (Pt 1), 59–66.

(6) Budihas, S. R.; Gorshkova, I.; Gaidamakov, S.; Wamiru, A.; Bona, M. K.; Parniak, M. A.; Crouch, R. J.; McMahon, J. B.; Beutler, J. A.; Le Grice, S. F. Selective inhibition of HIV-1 reverse transcriptase-associated ribonuclease H activity by hydroxylated tropolones. *Nucleic Acids Res.* **2005**, *33*, 1249–1256.

(7) Didierjean, J.; Isel, C.; Querre, F.; Mouscadet, J. F.; Aubertin, A. M.; Valnot, J. Y.; Piettre, S. R.; Marquet, R. Inhibition of human immunodeficiency virus type 1 reverse transcriptase, RNase H, and integrase activities by hydroxytropolones. *Antimicrob. Agents Chemother.* **2005**, *49*, 4884–4894.

(8) Dat, N. T.; Bae, K.; Wamiru, A.; McMahon, J. B.; Le Grice, S. F.; Bona, M.; Beutler, J. A.; Kim, Y. H. A dimeric lactone from Ardisia japonica with inhibitory activity for HIV-1 and HIV-2 ribonuclease H. *J. Nat. Prod.* **2007**, *70*, 839–841.

(9) Marchand, C.; Beutler, J. A.; Wamiru, A.; Budihas, S.; Mollmann, U.; Heinisch, L.; Mellors, J. W.; Le Grice, S. F.; Pommier, Y. Madurahydroxylactone derivatives as dual inhibitors of human immunodeficiency virus type 1 integrase and RNase H. *Antimicrob. Agents Chemother.* **2008**, *52*, 361–364.

(10) Takada, K.; Bermingham, A.; O′Keefe, B. R.; Wamiru, A.; Beutler, J. A.; Le Grice, S. F.; Lloyd, J.; Gustafson, K. R.; McMahon, J. B. An HIV RNase H inhibitory 1,3,4,5-tetragalloylapiitol from the African plant *Hylodendron gabunensis*. *J. Nat. Prod.* **2007**, *70*, 1647–1649.

(11) Kirschberg, T. A.; Balakrishnan, M.; Squires, N. H.; Barnes, T.; Brendza, K. M.; Chen, X.; Eisenberg, E. J.; Jin, W.; Kutty, N.; Leavitt, S.; Liclican, A.; Liu, Q.; Liu, X.; Mak, J.; Perry, J. K.; Wang, M.; Watkins, W. J.; Lansdon, E. B. RNase H active site inhibitors of human immunodeficiency virus type 1 reverse transcriptase: design, biochemical activity, and structural information. *J. Med. Chem.* **2009**, *52*, 5781–5784.

(12) Wendeler, M.; Lee, H. F.; Bermingham, A.; Miller, J. T.; Chertov, O.; Bona, M. K.; Baichoo, N. S.; Ehteshami, M.; Beutler, J.; O′Keefe, B. R.; Gotte, M.; Kvaratskhelia, M.; Le Grice, S. Vinylogous ureas as a novel class of inhibitors of reverse transcriptase-associated ribonuclease H activity. *ACS Chem. Biol.* **2008**, *3*, 635–644.

(13) Chung, S.; Wendeler, M.; Rausch, J. W.; Beilhartz, G.; Gotte, M.; O′Keefe, B. R.; Bermingham, A.; Beutler, J. A.; Liu, S. X.; Zhuang, X. W.; Le Grice, S. F. J. Structure−Activity Analysis of Vinylogous Urea Inhibitors of Human Immunodeficiency Virus-Encoded Ribonuclease H. *Antimicrob. Agents Chemother.* **2010**, *54*, 3913–3921.

(14) Di Grandi, M.; Olson, M.; Prashad, A. S.; Bebernitz, G.; Luckay, A.; Mullen, S.; Hu, Y. B.; Krishnamurthy, G.; Pitts, K.; O′Connell, J. Small molecule inhibitors of HIV RT Ribonuclease H. *Bioorg. Med. Chem. Lett.* **2010**, *20*, 398–402.

(15) Himmel, D. M.; Maegley, K. A.; Pauly, T. A.; Bauman, J. D.; Das, K.; Dharia, C.; Clark, A. D., Jr.; Ryan, K.; Hickey, M. J.; Love, R. A.; Hughes, S. H.; Bergqvist, S.; Arnold, E. Structure of HIV-1 reverse transcriptase with the inhibitor beta-thujaplicinol bound at the RNase H active site. *Structure* **2009**, *17*, 1625–1635.

(16) Himmel, D. M.; Sarafianos, S. G.; Dharmasena, S.; Hossain, M. M.; McCoy-Simandle, K.; Ilina, T.; Clark, A. D., Jr.; Knight, J. L.; Julias, J. G.; Clark, P. K.; Krogh-Jespersen, K.; Levy, R. M.; Hughes, S. H.; Parniak, M. A.; Arnold, E. HIV-1 reverse transcriptase structure with RNase H inhibitor dihydroxy benzoyl naphthyl hydrazone bound at a novel site. *ACS Chem. Biol.* **2006**, *1*, 702–712.

(17) Klumpp, K.; Mirzadegan, T. Recent progress in the design of small molecule inhibitors of HIV RNase H. *Curr. Pharm. Des.* **2006**, *12*, 1909–1922.

(18) Su, H. P.; Yan, Y. W.; Prasad, G. S.; Smith, R. F.; Daniels, C. L.; Abeywickrema, P. D.; Reid, J. C.; Loughran, H. M.; Kornienko, M.; Sharma, S.; Grobler, J. A.; Xu, B.; Sardana, V.; Allison, T. J.; Williams, P. D.; Darke, P. L.; Hazuda, D. J.; Munshi, S. Structural Basis for the Inhibition of RNase H Activity of HIV-1 Reverse Transcriptase by RNase H Active Site-Directed Inhibitors. *J. Virol.* **2010**, *84*, 7625–7633.

(19) Nakagawa, Y.; Tayama, K. Mechanism of mitochondrial dysfunction and cytotoxicity induced by tropolones in isolated rat hepatocytes. *Chem.-Biol. Interact.* **1998**, *116*, 45–60.

(20) Boone, L. R. Next-generation HIV-1 non-nucleoside reverse transcriptase inhibitors. *Curr. Opin. Invest. Drugs* **2006**, *7*, 128–135.

(21) Polonsky, J.; Beloeil, J. C.; Prange, T.; Pascard, C.; Jacquemin, H.; Donnelly, D. M. X.; Kenny, P. T. M. Manicol—a Sesquiterpenoid Hydroxytropolone from *Dulacia guianensis*—a Revised Structure (X-Ray-Analysis). *Tetrahedron* **1983**, *39*, 2647–2655.

(22) Yang, W.; Hendrickson, W. A.; Crouch, R. J.; Satow, Y. Structure of Ribonuclease-H Phased at 2-a Resolution by Mad Analysis of the Selenomethionyl Protein. *Science* **1990**, *249*, 1398–1405.

(23) Steitz, T. A.; Steitz, J. A. A general two-metal-ion mechanism for catalytic RNA. *Proc. Natl. Acad. Sci. U.S.A* **1993**, *90*, 6498–6502.

(24) Luzzati, V. Traitement Statistique Des Erreurs Dans La Determination Des Structures Cristallines. *Acta Crystallogr.* **1952**, *5*, 802–810.

(25) Baker, E. N. Hydrogen bonding in biological marcomolecules. In *International Tables for Crystallography, Vol. F: Crystallography of Biological Macromolecule*; Rossman, M. G., Arnold, E., Ed.; Kluwer Academic Publishers: Boston, 2001; pp 546−552.

(26) Bhattacharyya, R.; Saha, R. P.; Samanta, U.; Chakrabarti, P. Geometry of interaction of the histidine ring with other planar and basic residues. *J. Proteome Res.* **2003**, *2*, 255–263.

(27) Chakrabarti, P.; Bhattacharyya, R. Geometry of nonbonded interactions involving planar groups in proteins. *Prog. Biophys. Mol. Biol.* **2007**, *95*, 83–137.

(28) Schottel, B. L.; Chifotides, H. T.; Dunbar, K. R. Anion−pi interactions. *Chem. Soc. Rev.* **2008**, *37*, 68–83.

(29) Estarellas, C.; Frontera, A.; Quinonero, D.; Deya, P. M. Relevant Anion−pi Interactions in Biological Systems: The Case of Urate Oxidase. *Angew. Chem., Int. Ed.* **2011**, *50*, 415–418.

(30) Parniak, M. A.; Min, K. L.; Budihas, S. R.; Le Grice, S. F. J.; Beutler, J. A. A fluorescence-based high-throughput screening assay for inhibitors of human immunodeficiency virus-1 reverse transcriptase-associated ribonuclease H activity. *Anal. Biochem.* **2003**, *322*, 33–39.

(31) Gopalakrishnan, V.; Peliska, J. A.; Benkovic, S. J. Human immunodeficiency virus type 1 reverse transcriptase: spatial and temporal relationship between the polymerase and RNase H activities. *Proc. Natl. Acad. Sci. U.S.A* **1992**, *89*, 10763–10767.

(32) Hang, J. Q.; Li, Y.; Yang, Y.; Cammack, N.; Mirzadegan, T.; Klumpp, K. Substrate-dependent inhibition or stimulation of HIV RNase H activity by non-nucleoside reverse transcriptase inhibitors (NNRTIs). *Biochem. Biophys. Res. Commun.* **2007**, *352*, 341–350.

(33) Song, J. J.; Smith, S. K.; Hannon, G. J.; Joshua-Tor, L. Crystal structure of Argonaute and its implications for RISC slicer activity. *Science* **2004**, *305*, 1434–1437.

(34) Nikolenko, G. N.; Palmer, S.; Maldarelli, F.; Mellors, J. W.; Coffin, J. M.; Pathak, V. K. Mechanism for nucleoside analog-mediated abrogation of HIV-1 replication: balance between RNase H activity and nucleotide excision. *Proc. Natl. Acad. Sci. U.S.A.* **2005**, *102*, 2093–2098.

(35) Shaw-Reid, C. A.; Munshi, V.; Graham, P.; Wolfe, A.; Witmer, M.; Danzeisen, R.; Olsen, D. B.; Carroll, S. S.; Embrey, M.; Wai, J. S.; Miller, M. D.; Cole, J. L.; Hazuda, D. J. Inhibition of HIV-1 ribonuclease H by a novel diketo acid, 4-[5-(benzoylamino)thien-2-yl]-2,4-dioxobutanoic acid. *J. Biol. Chem.* **2003**, *278*, 2777–2780.

(36) Ratner, L.; Fisher, A.; Jagodzinski, L. L.; Mitsuya, H.; Liou, R. S.; Gallo, R. C.; Wongstaal, F. Complete Nucleotide-Sequences of Functional Clones of the Aids Virus. *AIDS Res. Hum. Retroviruses* **1987**, *3*, 57–69.

(37) Le Grice, S. F.; Gruninger-Leitch, F. Rapid purification of homodimer and heterodimer HIV-1 reverse transcriptase by metal chelate affinity chromatography. *Eur. J. Biochem.* **1990**, *187*, 307–14.

(38) Weislow, O. S.; Kiser, R.; Fine, D. L.; Bader, J.; Shoemaker, R. H.; Boyd, M. R. New soluble-formazan assay for HIV-1 cytopathic effects: application to high-flux screening of synthetic and natural products for AIDS-antiviral activity. *J. Natl. Cancer Inst.* **1989**, *81*, 577–586.

(39) Bauman, J. D.; Das, K.; Ho, W. C.; Baweja, M.; Himmel, D. M.; Clark, A. D., Jr.; Oren, D. A.; Boyer, P. L.; Hughes, S. H.; Shatkin, A. J.; Arnold, E. Crystal engineering of HIV-1 reverse transcriptase for structure-based drug design. *Nucleic Acids Res.* **2008**, *36*, 5083–5092.

(40) Clark, A. D., Jr.; Jacobo-Molina, A.; Clark, P.; Hughes, S. H.; Arnold, E. Crystallization of human immunodeficiency virus type 1 reverse transcriptase with and without nucleic acid substrates, inhibitors, and an antibody Fab fragment. *Methods Enzymol.* **1995**, *262*, 171–185.

(41) Otwinowski, Z.; Minor, W. DENZO and SCALEPACK. In *International Tables for Crystallography, Vol. F: Crystallography of Biological Macromolecules*, 1st ed.; Rossman, M. G., Arnold, E., Ed.; Kluwer Academic Publishers: Boston, 2001; pp 226−235.

(42) Otwinowski, Z.; Minor, W. Processing of X-Ray Diffraction Data Collected in Oscillation Mode. In *Methods in Enzymology: Marcomolecular Crystallography Part A*, 1st ed.; Charles, W., Carter, J., Sweet, R. M., Ed.; Academic Press, Inc.: New York, 1997; Vol. 276, pp 307−326.

(43) Read, R. J. Pushing the boundaries of molecular replacement with maximum likelihood. *Acta Crystallogr., Sect. D: Biol. Crystallogr.* **2001**, *57*, 1373–1382.

(44) Das, K.; Bauman, J. D.; Clark, A. D., Jr.; Frenkel, Y. V.; Lewi, P. J.; Shatkin, A. J.; Hughes, S. H.; Arnold, E. High-resolution structures of HIV-1 reverse transcriptase/TMC278 complexes: strategic flexibility explains potency against resistance mutations. *Proc. Natl. Acad. Sci. U.S.A* **2008**, *105*, 1466–1471.

(45) Jones, T. A.; Zou, J. Y.; Cowan, S. W.; Kjeldgaard, M. Improved methods for building protein models in electron density maps and the location of errors in these models. *Acta Crystallogr., Sect. A: Found. Crystallogr.* **1991**, *47* (Pt 2), 110–119.

(46) Emsley, P.; Cowtan, K. Coot: model-building tools for molecular graphics. *Acta Crystallogr., Sect. D: Biol. Crystallogr.* **2004**, *60*, 2126–2132.

(47) Brunger, A. T.; Adams, P. D.; Clore, G. M.; DeLano, W. L.; Gros, P.; Grosse-Kunstleve, R. W.; Jiang, J. S.; Kuszewski, J.; Nilges, M.; Pannu, N. S.; Read, R. J.; Rice, L. M.; Simonson, T.; Warren, G. L. Crystallography & NMR system: A new software suite for macromolecular structure determination. *Acta Crystallogr., Sect. D: Biol. Crystallogr.* **1998**, *54*, 905–921.

(48) Perrakis, A.; Harkiolaki, M.; Wilson, K. S.; Lamzin, V. S. ARP/wARP and molecular replacement. *Acta Crystallogr., Sect. D: Biol. Crystallogr.* **2001**, *57*, 1445–1450.

(49) Lamzin, V. S.; Perrakis, A.; Wilson, K. S. The ARP/wARP Suite for Automated Construction and Refinement of Protein Models. In *International Tables for Crystallography, Vol. F: Crystallography of Biological Macromolecules*, 1st ed.; Rossman, M. G., Arnold, E., Ed.; Kluwer Academic Publishers: Boston, 2001; pp 720−722.

(50) Perrakis, A.; Sixma, T. K.; Wilson, K. S.; Lamzin, V. S. wARP: improvement and extension of crystallographic phases by weighted averaging of multiple-refined dummy atomic models. *Acta Crystallogr., Sect. D: Biol. Crystallogr.* **1997**, *53*, 448–455.

(51) Murshudov, G. N.; Vagin, A. A.; Dodson, E. J. Refinement of macromolecular structures by the maximum-likelihood method. *Acta Crystallogr., Sect. D: Biol. Crystallogr.* **1997**, *53*, 240–255.

(52) Lamzin, V. S.; Wilson, K. S. Automated refinement of protein models. *Acta Crystallogr., Sect. D: Biol. Crystallogr.* **1993**, *49*, 129–147.

(53) Jacobo-Molina, A.; Ding, J.; Nanni, R. G.; Clark, A. D., Jr.; Lu, X.; Tantillo, C.; Williams, R. L.; Kamer, G.; Ferris, A. L.; Clark, P.; Hizi, A.; Hughes, S. H.; Arnold, E. Crystal structure of human immunodeficiency virus type 1 reverse transcriptase complexed with double-stranded DNA at 3.0 A resolution shows bent DNA. *Proc. Natl. Acad. Sci. U.S.A* **1993**, *90*, 6320–6324.